PHYSICAL REVIEW B **95**, 121410(R) (2017)

Realization of quantum anomalous Hall effect in graphene from *n*-*p* codoping-induced stable atomic adsorption

Xinzhou Deng,[1,2] Shifei Qi,[1,3] Yulei Han,[1,2] Kunhua Zhang,[1,2] Xiaohong Xu,[3,*] and Zhenhua Qiao[1,2,†]

[1]*ICQD, Hefei National Laboratory for Physical Sciences at Microscale, and Synergetic Innovation Center of Quantum Information and Quantum Physics, University of Science and Technology of China, Hefei, Anhui 230026, China*

[2]*CAS Key Laboratory of Strongly-Coupled Quantum Matter Physics, and Department of Physics, University of Science and Technology of China, Hefei, Anhui 230026, China*

[3]*School of Chemistry and Materials Science, Shanxi Normal University, Linfen, Shanxi 041004, China*

(Received 22 September 2016; revised manuscript received 29 January 2017; published 29 March 2017)

Using first-principles calculation methods, we study the possibility of realizing a quantum anomalous Hall effect in graphene from stable 3*d* atomic adsorption via a charge-compensated *n*-*p* codoping scheme. As concrete examples, we show that long-range ferromagnetism can be established by codoping 3*d* transition metal and boron atoms, but only the Ni codopants can open up a global bulk gap to harbor the quantum anomalous Hall effect. Our estimated ferromagnetic Curie transition temperature can reach over 10 K for various codoping concentrations.

DOI: 10.1103/PhysRevB.95.121410

Introduction. The quantum anomalous Hall effect (QAHE) is a quantized response of transverse charge current to an electric field in the absence of magnetic field [1–4]. It originates from the joint effect of spin-orbit coupling and local magnetization. The presence of linear Dirac dispersion has made both graphene [5] and topological insulators (TIs) [6,7] ideal platforms to explore QAHE. Comparing with graphene, TIs show great superiority because of their intrinsic spin-orbit couplings, which indicate that the only condition to realize QAHE in TIs is to break time-reversal invariance. By doping magnetic atoms into TI thin films [e.g., doping Cr/V atoms in $(Bi,Sb)_2Te_3$], QAHE has been theoretically proposed [8,9] and later experimentally observed at extremely low temperatures (e.g., <100 mK) [10–16]. A charge-compensated *n*-*p* codoping scheme was adopted to increase the QAHE observation temperature in TI thin films, e.g., a temperature over 50 K can be achieved by codoping vanadium and iodine atoms into Sb_2Te_3 thin films [17].

Alternatively, although graphene is nonmagnetic and exhibits extremely weak spin-orbit coupling [5,18–20], it still attracts broad attention to produce QAHE because of its superior electronic properties and broad perspective for future industry-scale applications. In Refs. [21–24], it was theoretically shown that Rashba spin-orbit coupling together with ferromagnetism leads to the formation of QAHE in graphene by periodically doping magnetic atoms. However, precise control of the doping position has not been achieved in current experimental techniques. This makes this QAHE proposal unrealistic because of the potentially induced intervalley scattering during nonperiodic doping schemes. Strikingly, a followup study [25] showed that a random distribution of magnetic dopants in graphene can greatly eliminate intervalley scattering. Subsequent studies from both theoretical and experimental points of view showed that magnetic atoms in graphene tend to nucleate into clusters on graphene owing to the small binding energies [26,27]. After some efforts, a rewarding approach was theoretically proposed to realize QAHE by placing graphene on magnetic insulator thin films [28,29]. Soon, it was experimentally reported that a sizable AHE can be observed in graphene by considering $Y_3Fe_5O_{12}$ (YIG) magnetic thin films [30]. Such a scheme can lead to considerable ferromagnetism in graphene, but extremely weak Rashba spin-orbit coupling [30,31]. The fundamental reason for the weak Rashba spin-orbit coupling arises from the large separation ($\sim$2.5–3 Å; see Refs. [28,29]) between graphene and the magnetic insulating substrate due to a weak van der Waals interaction, which shows a clear contrast with the chemical interaction in the atomic adsorption situation ($\sim$1.6 Å; see Refs. [21,22,24]). Thus, extremely weak Rashba spin-orbit coupling is the only ingredient to hinder the realization of QAHE.

To our knowledge, the most rewarding approach to increase Rashba spin-orbit coupling in graphene is to design a stable atomic adsorption scheme. Inspired by the advantages of manipulating band gaps from the *n*-*p* codoping method [32–39] and the successful fabrication of boron (B)-substituted graphene [40], we present a systematic investigation on the possible realization of QAHE in graphene by utilizing the *n*-*p* codoping technique. As examples, we take 3*d* transition metal atoms as *n*-type dopants that are adsorbed on top of graphene and B atoms as *p*-type dopants that substitute carbon atoms. We show that although the magnetic states for most 3*d* adatoms (except Cr and Mn) show a Ruderman-Kittel-Kasuya-Yosida (RKKY)-type spatial fluctuation, only V or Ni atoms can exhibit long-range ferromagnetic orders in B-substituted graphene. When spin-orbit coupling is further invoked, we find that only Ni-B codoping can open up a global band gap that harbors the QAHE. This is completely distinct from the situation of single-element Ni-adsorbed graphene [22,41,42] that induces vanishing ferromagnetism arising from the electron redistribution, i.e., $3d^8 4s^2 \rightarrow 3d^{10} 4s^0$. We further show the dependence of the QAHE gap on the codoping concentration.

Computational methods. First-principles calculations were performed within the framework of density functional theory using the projected augmented-wave method [43] as implemented in the Vienna *ab initio* simulation package [44–46]. The generalized gradient approximation [47] of Perdew-Burke-Ernzerhof [48] was adopted to treat the exchange correlation interactions. To avoid intervalley scattering in the

*xuxh@dns.sxnu.edu.cn
†qiao@ustc.edu.cn

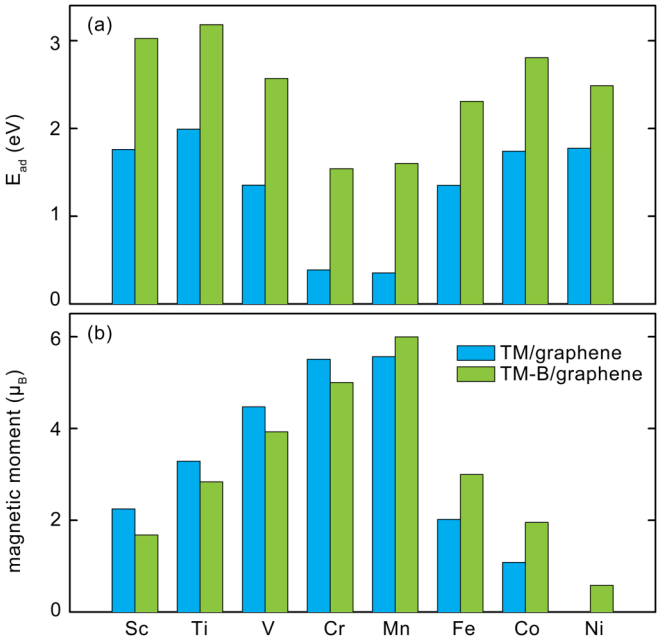

FIG. 1. (a) Adsorption energy and (b) magnetic moment of 3*d* TM adatoms on pristine graphene (blue) and B-codoped graphene (green).

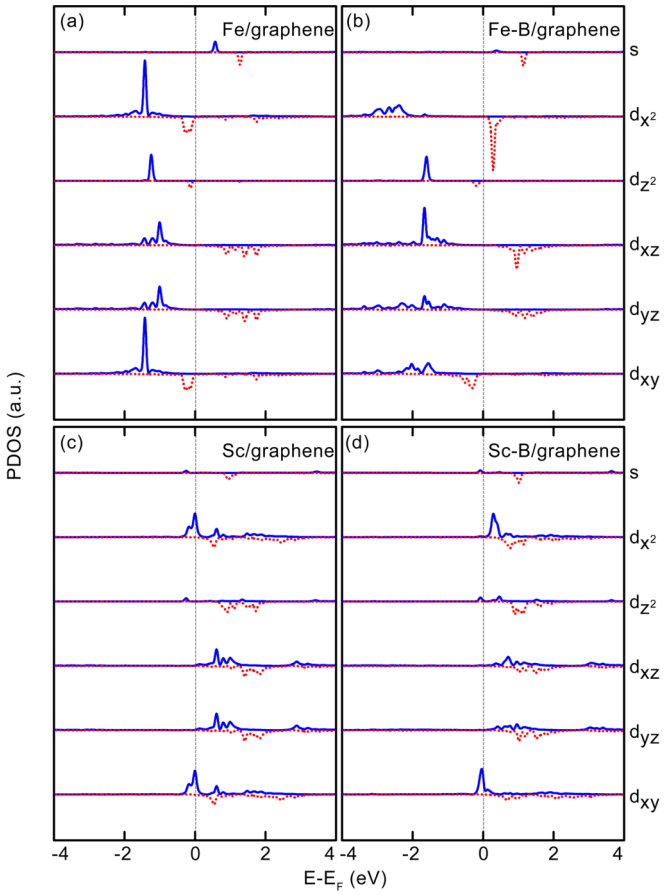

FIG. 2. Orbital-resolved DOS of Fe adatom on (a) pristine graphene and (b) B-codoped graphene. Orbital-resolved DOS of Sc adatom on (c) pristine graphene and (d) B-codoped graphene. Blue solid lines: majority spin; red dotted lines: minority spin.

codoping scheme, an 8×8 graphene supercell was adopted. A vacuum space of 20 Å between two graphene layers was set to avoid spurious interactions between periodic images. The kinetic energy cutoff and the energy convergence threshold were set to be 400 and 10^{-4} eV, respectively. The atomic structures were fully relaxed until the Hellmann-Feynman force on each ion was less than 0.02 eV/Å. The Gaussian smearing method with a smearing width of 0.1 eV and a *k*-mesh point grid of $3 \times 3 \times 1$ was adopted during the structural relaxation. A *k*-mesh point of $5 \times 5 \times 1$ was used for the total energy estimation, while a $11 \times 11 \times 1$ *k*-mesh point mesh was used in calculating the density of states.

Adsorption analysis. We begin by revisiting the single-element adsorbed graphene. Previous studies showed that most 3*d* metal adatoms favor a hollow position [22,49,50]. Thus, the corresponding adsorption energy E_{ad} can be defined as

$$E_{ad} = E_{TM} + E_{Gra} - E_{Tot},$$

where E_{TM}, E_{Gra}, and E_{Tot} are respectively the energies of the isolated transition metal atoms, pristine graphene, and the atom-adsorbed graphene. The blue bars in Fig. 1(a) display the adsorption energy of only metal atom-adsorbed graphene, which agrees well with previous studies in the range of 0.4–1.9 eV [22,51,52]. The relatively weak adsorption energy cannot prevent the fast migration of adatom clustering when other adatoms are further adsorbed on graphene. To overcome the difficulty of forming a dilute adatom distribution, an *n*-*p* codoping scheme was proposed in a previous work where codoping with B atoms is able to significantly suppress those undesirable effects and the metal adatoms are closely located near the substituted B positions due to a strong electrostatic attraction [39]. When B codopants are considered, as displayed by the green bars in Fig. 1(a), the adsorption energy exhibits a ∼1 eV enhancement compared with single-element doping, which can effectively prevent adatom migration and clustering on B-substituted graphene. Based on the Arrhenius equation, the room temperature corresponds to an adsorption energy of $E_{ad} \sim 0.75$ eV. Thus, the estimated stable temperature of transition metal adatoms on B-doped graphene is within the range of 617–1273 K, which is larger than that (142–797 K) of only adsorbing transition metal atoms on graphene. This indicates that *n*-*p* codoping adsorption on graphene is more stable above room temperature in this study. This codoping scheme provides a basic material structure with a stable dilute distribution of adatoms in graphene.

We now investigate the magnetic property of the codoped graphene system. In Fig. 1(b), one can find that the resulting magnetic moments of Sc, Ti, V, and Cr adatoms on graphene decrease when B atoms are codoped, while those of Mn, Fe, Co, and Ni adatoms increase after B codoping. Below, we take Fe and Sc atoms as examples to analyze the variance of the magnetic moments after B codoping. Figure 2 displays the orbital-resolved density of states (DOS) of Fe and Sc adatoms on pristine and B-doped graphene, respectively. Compared with the pristine graphene, *p*-doped B-substituted graphene weakens the hybridization effect of lowering the 3*d* orbital energies, therefore hindering the charge transfer from 4*s* electrons to 3*d* orbitals. This makes the magnetic moments

of the transition metal adatoms smaller (i.e., Sc, Ti, V) or larger (i.e., Fe, Co, Ni) than those on pristine graphene (see Fig. 1), while Cr and Mn atoms contribute their 4*s* electrons to *p*-doped graphene, making its magnetic moment exactly equal to $5\mu_B$ and $6\mu_B$, respectively. The orbital-resolved density of states presented in Fig. 2 further confirms this physical mechanism: When the Fe atom is adsorbed on pristine graphene [see Fig. 2(a)], electrons fully occupy five spin-up 3*d* orbitals and three spin-down 3*d* orbitals; after B codoping, electrons fully occupy five spin-up 3*d* orbitals but only two spin-down 3d orbitals [see Fig. 2(b)], resulting in an increase of the magnetic moment from $2\mu_B$ to $3\mu_B$. For Sc adatoms, there is one spin-up 3*d* orbital fully occupied and two spin-up 3*d* orbitals partially occupied in the case of pristine graphene [see Fig. 2(c)], while there is only one spin-up 3*d* orbital fully occupied and one spin-up 3*d* orbital partially occupied in the case of B-substituted graphene [see Fig. 2(d)], leading to a smaller magnetic moment.

The above results show that the codoping approach can indeed stabilize the dilute distribution of metal adatoms with B substitution in graphene, and the magnetic moments of Mn, Fe, Co, and Ni significantly increase while those of Sc, Ti, V, and Cr remain relatively large. Now we further study the magnetic interactions between two codopants (metal atom and B) pairs by setting them in an 8×8 graphene supercell. As displayed in Fig. 3(a), one metal adatom is located at the H_0 site pairing with a B dopant at the S_0 site, and the second metal adatom moves from H_1 to H_7 accompanied by the movement of its nearest-neighbor B codopant. Figure 3(b) summarizes the energy difference between the ferromagnetic and antiferromagnetic states of the two transition metal atoms at given separations. We find that the first to third nearest-neighbor configurations are unstable for Cr and Mn adatoms, because the attraction between two Cr or Mn adatoms is surprisingly large to form clusters even though their corresponding adsorption energies increase after codoping with B atoms. The second/third nearest-neighbor configurations of Sc, Ti, V and the second nearest-neighbor configurations of Fe, Co, Ni are also unstable, with adatoms always tending to form the first nearest-neighbor configuration.

The strong ferromagnetism or antiferromagnetism coupling at the first nearest-neighbor distance for Sc, Ti, V, Fe, and Co is closely related to the direct exchange interaction because their first nearest-neighbor distances are approximately equal to the first nearest-neighbor distances in their respective bulk crystals, while Ni adatoms exhibit a weaker coupling energy because of their small magnetic moments. However, most of them present a RKKY-like long-range magnetic interaction, except for Cr and Mn that display paramagnetism. One can observe that only V-B and Ni-B codoped graphene systems exhibit ferromagnetism at some longer adatom-adatom distances. This indicates the potential long-range ferromagnetic order in these systems.

Ni-B codoping. From the above analysis, we find that both V-B and Ni-B codoping may realize diluted ferromagnetism in graphene. Then we study whether the QAHE can be realized in V-B and Ni-B codoped graphene. Our further calculations show that the introduction of spin-orbit coupling in V-B codoped graphene does not open a bulk gap in any codoping concentration. Therefore, below we only consider

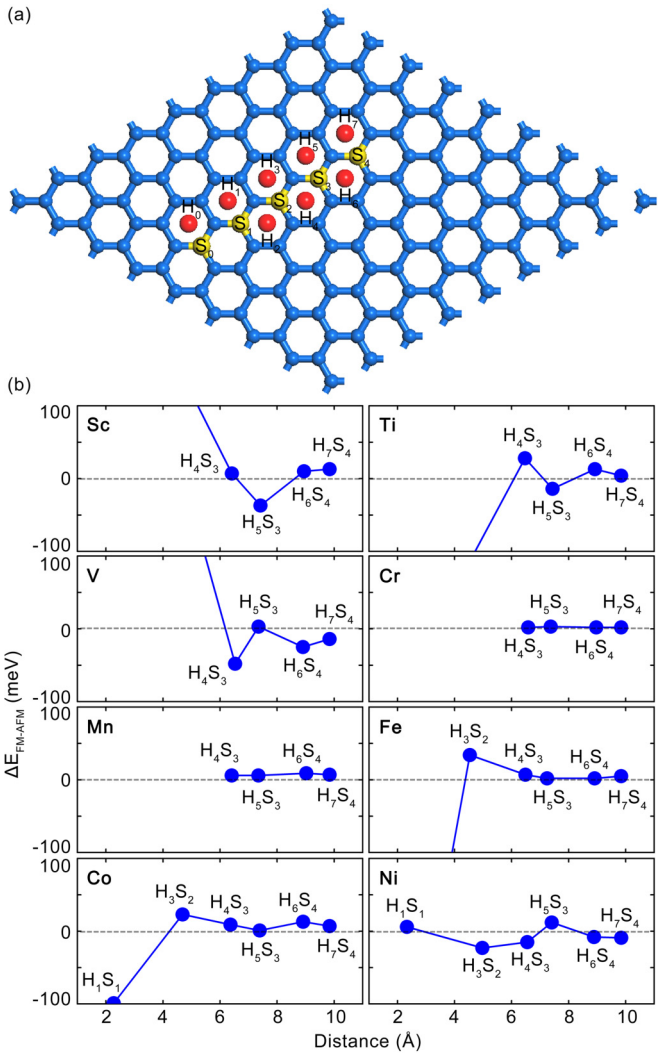

FIG. 3. (a) An 8×8 supercell of graphene. H_0–H_7 and S_0–S_4 represent sites for the transition metal adatoms and substitutional B dopants, respectively. (b) Magnetic coupling between two codopant pairs at different distances. One pair is fixed at H_0S_0 and the other moves from H_1S_1 to H_7S_4, as illustrated in (a).

the Ni-B codoped graphene. We first investigate the band structures of Ni-B codoped graphene at different codoping concentrations. By codoping two, four, and six Ni-B pairs in an 8×8 supercell of graphene, one can get corresponding concentrations of 1.6%, 3.1%, and 4.7%, respectively. Due to the equal probability of different sublattices in graphene to be substituted experimentally, the amount of B dopants in the A/B sublattice is set to be identical. Figure 4(a) displays the band structure of codoping six Ni-B pairs in the 8×8 supercell of graphene, with bulk band gaps opening near the K and K' valleys when spin-orbit coupling is invoked. For the three different codoping concentrations mentioned above, the resulting bulk gaps are respectively 4, 8, and 10 meV [see Fig. 4(c)], suggesting a gap tunability by controlling the codoping concentration. Another obvious finding is that Fermi levels lie outside the gaps for all concentrations and the shift of the valence band maximum from the Fermi level enlarges with an increase of doping concentration, as plotted in Fig. 4(d),

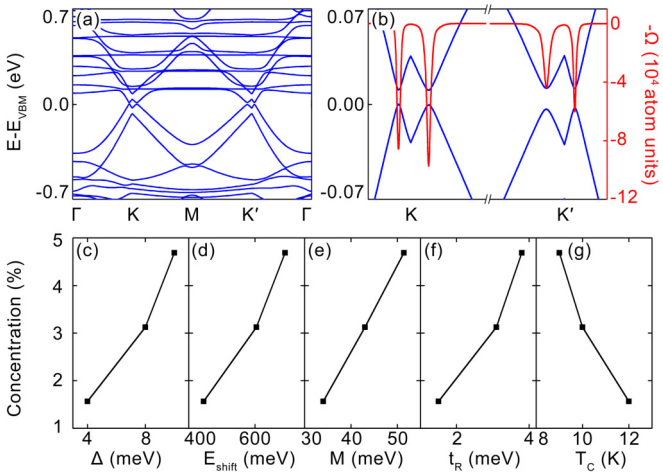

FIG. 4. (a) Full band structure of six Ni-B codoping pairs in the 8×8 supercell of graphene along the high symmetry lines. (b) Zoom in of the bands around the K and K' Dirac points. The red line represents the Berry curvature. (c) The band gap Δ, (d) shift of valence band maximum from Fermi level E_{shift}, (e) exchange field M, (f) Rashba spin-orbit coupling strength t_R, and (g) simulated Curie temperature T_C as a function of Ni-B pair concentration.

because of the p-doping effect of B atoms. To realize the insulating nature, artificial adjustment is required to tune the Fermi levels into the bulk gaps, e.g., by applying a gate voltage or tuning the ratio between the B and Ni dopants.

So far, we have shown that Ni-B codoped graphene can form long-range ferromagnetism and the presence of spin-orbit coupling can further open up a band gap. Below, we investigate whether such a band gap can harbor the QAHE via a Chern number calculation, which can be obtained by integrating the Berry curvatures of the occupied valence bands using the expression [53,54]

$$\Omega(\boldsymbol{k}) = -\sum_{n} f_n \sum_{n' \neq n} \frac{2\,\mathrm{Im}\langle\psi_{nk}|v_x|\psi_{n'k}\rangle\langle\psi_{n'k}|v_y|\psi_{nk}\rangle}{(E_{n'} - E_n)^2},$$

where n, E_n, and ψ_{nk} are the band index, eigenvalue, and eigenstate of the nth band, respectively. $v_{x,y} = \partial E/\partial k_{x,y}$ are the velocity operators along the x and y directions within the film plane, and $f_n = 1$ for all n bands below the band gap. Our calculation finds that this gap can host the QAHE. As an example, Fig. 4(b) displays the Berry curvature distribution along the high symmetry lines with large negative peaks appearing near the K and K' valleys and vanishing elsewhere, demonstrating a nonzero Hall conductance. The Chern number can be obtained by integrating the Berry curvatures $\Omega(\boldsymbol{k})$ over the first Brillouin zone using the equation

$$\mathcal{C} = \frac{1}{2\pi}\int_{\mathrm{BZ}} d^2k\,\Omega(\boldsymbol{k}),$$

which is numerically calculated to be $\mathcal{C} = 2$ in our study. This guarantees the formation of QAHE in Ni-B codoped graphene.

From a former theory [21], it is known that both the ferromagnetic exchange field (M) and Rashba spin-orbit coupling (t_R) play crucial roles in realizing graphene-based QAHE. By fitting our band structures around the K and K' valleys, we can extract the corresponding parameters M and t_R. Figures 4(e) and 4(f) display the dependence of exchange field and Rashba spin-orbit coupling on the codoping concentration. One can see that with increasing doping concentration, both M and t_R increase almost linearly, which agrees with the band gap increasing from our first-principles calculations.

Curie temperature. The experimental observation temperature is determined by the lower limit of the bulk band gap and ferromagnetic Curie temperature T_C. We calculate the Curie temperature (T_C) by using the Monte Carlo method [55,56] as applied to the diluted magnetic semiconductors within the classical Heisenberg model,

$$H = -\sum_{i,j} J_{ij}\mathbf{S}_i \cdot \mathbf{S}_j,$$

where J_{ij} is the magnetic coupling constant between moments i and j, and $\mathbf{S}_i$ is a unit vector representing the direction of spin i. The magnetic coupling strength J for the pair of magnetic atoms is obtained from the energy difference between antiferromagnetic and ferromagnetic configurations ($J = E_{\mathrm{AFM}} - E_{\mathrm{FM}}$). The thermodynamic magnetization per atom and the susceptibility are respectively calculated by

$$m(T) = \left\langle \left[\left(\sum_i \mathbf{S}_i^x\right)^2 + \left(\sum_i \mathbf{S}_i^y\right)^2 + \left(\sum_i \mathbf{S}_i^z\right)^2 \right]^{1/2} \right\rangle \Big/ N,$$

$$\chi = N(\langle m^2\rangle - \langle m\rangle^2)/T,$$

where N is the number of magnetic atoms. In a Monte Carlo simulation, we consider a 12×12 graphene supercell and average the normalized magnetization and susceptibility by collecting 10 000 configurations with randomly distributed Ni-B pairs. At a given temperature, the first 10 000 Monter Carlo steps are used for relaxation, and thermodynamic quantities are calculated in the following 10 000 steps. By analyzing the simulated susceptibility χ as a function of temperature for graphene with 1.6%, 3.1%, and 4.7% Ni-B codoping, the T_C's are estimated to be 12, 10, and 9 K, respectively, which are highlighted by susceptibility peaks. Figure 4(g) displays that the ferromagnetic Curie temperature T_C does not grow with the codoping concentration because of the dominating antiferromagnetic state at the H_1S_1 configuration as displayed in Fig. 3(b).

Conclusions. In summary, we systematically investigated the adsorption of $3d$ transition metal atoms from Sc to Ni on B-doped graphene using first-principles calculation methods. Comparing with the adsorption on pristine graphene, we found that the $3d$ transition metal atoms have a larger adsorption energy on B-codoped graphene, thus significantly suppressing adatom migration and clustering. After investigating the magnetic states, we found that most exhibit RKKY magnetic fluctuations, but only V and Ni can form long-range ferromagnetism on B-doped graphene. Moreover, a Berry curvature calculation confirms that only Ni-B codoped graphene can open a band gap to harbor the QAHE, and the nontrivial band gap can be tuned by the adsorption concentration. The estimated ferromagnetic Curie temperature can reach over 10 K for various codoping concentrations.

Details of the calculations are available in the Supplemental Material [57].

Acknowledgments. This work was financially supported by the National Key R & D Program (Grant No. 2016YFA0301700), the National Natural Science Foundation of China (Grants No. 11474265 and No. 61434002), and the China Government Youth 1000-Plan Talent Program. The Supercomputing Center of USTC is gratefully acknowledged for high-performance computing assistance.

[1] F. D. M. Haldane, Phys. Rev. Lett. **61**, 2015 (1988).
[2] H. Weng, R. Yu, X. Hu, X. Dai, and Z. Fang, Adv. Phys. **64**, 227 (2015).
[3] Y. F. Ren, Z. H. Qiao, and Q. Niu, Rep. Prog. Phys. **79**, 066501 (2016).
[4] C.-X. Liu, S.-C. Zhang, and X.-L. Qi, Annu. Rev. Condens. Matter Phys. **7**, 301 (2016).
[5] A. H. Castro Neto, F. Guinea, N. M. R. Peres, K. S. Novoselov, and A. K. Geim, Rev. Mod. Phys. **81**, 109 (2009).
[6] M. Z. Hasan and C. L. Kane, Rev. Mod. Phys. **82**, 3045 (2010).
[7] X. L. Qi and S. C. Zhang, Rev. Mod. Phys. **83**, 1057 (2011).
[8] R. Yu, W. Zhang, H.-J. Zhang, S.-C. Zhang, X. Dai, and Z. Fang, Science **329**, 61 (2010).
[9] H. Jiang, Z. H. Qiao, H. W. Liu, and Q. Niu, Phys. Rev. B **85**, 045445 (2012).
[10] C.-Z. Chang, J. S. Zhang, X. Feng, J. Shen, Z. C. Zhang, M. Guo, K. Li, Y. Ou, P. Wei, L.-L. Wang, Z.-Q. Ji, Y. Feng, S. H. Ji, X. Chen, J. F. Jia, X. Dai, Z. Fang, S.-C. Zhang, K. He, Y. Y. Wang, L. Lu, X.-C. Ma, and Q.-K. Xue, Science **340**, 167 (2013).
[11] J. G. Checkelsky, R. Yoshimi, A. Tsukazaki, K. S. Takahashi, Y. Kozuka, J. Falson, M. Kawasaki, and Y. Tokura, Nat. Phys. **10**, 731 (2014).
[12] X. Kou, S.-T. Guo, Y. Fan, L. Pan, M. Lang, Y. Jiang, Q. Shao, T. Nie, K. Murata, J. Tang, Y. Wang, L. He, T.-K. Lee, W.-L. Lee, and K. L. Wang, Phys. Rev. Lett. **113**, 137201 (2014).
[13] C.-Z. Chang, W. Zhao, D. Y. Kim, H. Zhang, B. A. Assaf, D. Heiman, S.-C. Zhang, C. Liu, M. H. W. Chan, and J. S. Moodera, Nat. Mater. **14**, 473 (2015).
[14] A. J. Bestwick, E. J. Fox, X. Kou, L. Pan, K. L. Wang, and D. Goldhaber-Gordon, Phys. Rev. Lett. **114**, 187201 (2015).
[15] X. Kou, L. Pan, J. Wang, Y. Fan, E. S. Choi, W. L. Lee, and K. L. Wang, Nat. Commun. **6**, 8474 (2015).
[16] M. Mogi, R. Yoshimi, A. Tsukazaki, K. Yasuda, Y. Kozuka, K. S. Takahashi, and Y. Tokura, Appl. Phys. Lett. **107**, 182401 (2015).
[17] S. F. Qi, Z. H. Qiao, X. Z. Deng, E. D. Cubuk, H. Chen, W. G. Zhu, E. Kaxiras, S. B. Zhang, X. H. Xu, and Z. Y. Zhang, Phys. Rev. Lett. **117**, 056804 (2016).
[18] H. Min, J. E. Hill, N. A. Sinitsyn, B. R. Sahu, L. Kleinman, and A. H. MacDonald, Phys. Rev. B **74**, 165310 (2006).
[19] Y. G. Yao, F. Ye, X.-L. Qi, S.-C. Zhang, and Z. Fang, Phys. Rev. B **75**, 041401 (2007).
[20] M. Gmitra, S. Konschuh, C. Ertler, C. Ambrosch-Draxl, and J. Fabian, Phys. Rev. B **80**, 235431 (2009).
[21] Z. H. Qiao, S. A. Yang, W. X. Feng, W.-K. Tse, J. Ding, Y. G. Yao, J. Wang, and Q. Niu, Phys. Rev. B **82**, 161414 (2010); Z. H. Qiao, H. Jiang, X. Li, Y. G. Yao, and Q. Niu, *ibid.* **85**, 115439 (2012).
[22] J. Ding, Z. H. Qiao, W. X. Feng, Y. G. Yao, and Q. Niu, Phys. Rev. B **84**, 195444 (2011).
[23] W.-K. Tse, Z. H. Qiao, Y. G. Yao, A. H. MacDonald, and Q. Niu, Phys. Rev. B **83**, 155447 (2011).
[24] H. B. Zhang, C. Lazo, S. Blugel, S. Heinze, and Y. Mokrousov, Phys. Rev. Lett. **108**, 056802 (2012).
[25] H. Jiang, Z. Qiao, H. Liu, J. Shi, and Q. Niu, Phys. Rev. Lett. **109**, 116803 (2012).
[26] T. Eelbo, M. Waśniowska, P. Thakur, M. Gyamfi, B. Sachs, T. O. Wehling, S. Forti, U. Starke, C. Tieg, A. I. Lichtenstein, and R. Wiesendanger, Phys. Rev. Lett. **110**, 136804 (2013).
[27] H. Chen, Q. Niu, Z. Y. Zhang, and A. H. MacDonald, Phys. Rev. B **87**, 144410 (2013).
[28] Z. H. Qiao, W. Ren, H. Chen, L. Bellaiche, Z. Y. Zhang, A. H. MacDonald, and Q. Niu, Phys. Rev. Lett. **112**, 116404 (2014).
[29] J. Zhang, B. Zhao, Y. G. Yao, and Z. Q. Yang, Sci. Rep. **5**, 10629 (2015).
[30] Z. Wang, C. Tang, R. Sachs, Y. Barlas, and J. Shi, Phys. Rev. Lett. **114**, 016603 (2015).
[31] G. H. Cheng, L. M. Wei, L. Cheng, H. X. Liang, X. Q. Zhang, H. Li, G. L. Yu, and C. G. Zeng, Appl. Phys. Lett. **105**, 133111 (2014).
[32] T. Yamamoto and H. Katayama-Yoshida, Jpn. J. Appl. Phys. **38**, L166 (1999).
[33] L. G. Wang and A. Zunger, Phys. Rev. Lett. **90**, 256401 (2003).
[34] Y. Gai, J. B. Li, S.-S. Li, J.-B. Xia, and S.-H. Wei, Phys. Rev. Lett. **102**, 036402 (2009).
[35] W. Zhu, X. Qiu, V. Iancu, X.-Q. Chen, H. Pan, W. Wang, N. M. Dimitrijevic, T. Rajh, H. M. Meyer III, M. P. Paranthaman, G. M. Stocks, H. H. Weitering, B. Gu, G. Eres, and Z. Zhang, Phys. Rev. Lett. **103**, 226401 (2009).
[36] X. H. Xu, H. J. Blythe, M. Ziese, A. J. Behan, J. R. Neal, A. Mokhtari, R. M. Ibrahim, A. M. Fox, and G. A. Gehring, New J. Phys. **8**, 135 (2006).
[37] W. G. Zhu, Z. Y. Zhang, and E. Kaxiras, Phys. Rev. Lett. **100**, 027205 (2008).
[38] X. Y. Zhang, S. F. Qi, and X. H. Xu, Carbon **95**, 65 (2015).
[39] S. F. Qi, H. Chen, X. H. Xu, and Z. Y. Zhang, Carbon **61**, 609 (2013).
[40] S. Agnoli and M. Favaro, J. Mater. Chem. A **4**, 5002 (2016)
[41] K. T. Chan, J. B. Neaton, and M. L. Cohen, Phys. Rev. B **77**, 235430 (2008).
[42] H. Sevinçli, M. Topsakal, E. Durgun, and S. Ciraci, Phys. Rev. B **77**, 195434 (2008).
[43] P. E. Blöchl, Phys. Rev. B **50**, 17953 (1994).
[44] G. Kresse and J. Furthmüller, Comput. Mater. Sci. **6**, 15 (1996).
[45] G. Kresse and J. Furthmüller, Phys. Rev. B **54**, 11169 (1996).
[46] G. Kresse and D. Joubert, Phys. Rev. B **59**, 1758 (1999).
[47] J. P. Perdew, J. A. Chevary, S. H. Vosko, K. A. Jackson, M. R. Pederson, D. J. Singh, and C. Fiolhais, Phys. Rev. B **46**, 6671 (1992).
[48] J. P. Perdew, K. Burke, and M. Ernzerhof, Phys. Rev. Lett. **77**, 3865 (1996).
[49] M. Manadé, F. Viñes, and F. Illas, Carbon **95**, 525 (2015).

[50] B. Uchoa, C.-Y. Lin, and A. H. Castro Neto, Phys. Rev. B **77**, 035420 (2008).

[51] H. Johll, H. C. Kang, and E. S. Tok, Phys. Rev. B **79**, 245416 (2009).

[52] R. Q. Zhang, Y. F. Luo, S. F. Qi, and X. H. Xu, Appl. Surf. Sci. **305**, 768 (2014).

[53] Y. G. Yao, L. Kleinman, A. H. MacDonald, J. Sinova, T. Jungwirth, D.-S. Wang, E. Wang, and Q. Niu, Phys. Rev. Lett. **92**, 037204 (2004).

[54] D. Xiao, M.-C. Chang, and Q. Niu, Rev. Mod. Phys. **82**, 1959 (2010).

[55] H. Chen, W. Zhu, E. Kaxiras, and Z. Zhang, Phys. Rev. B **79**, 235202 (2009).

[56] Q. Y. Wu, Z. G. Chen, R. Wu, G. G. Xu, Z. G. Huang, F. M. Zhang, and Y. W. Du, Solid State Commun. **142**, 242 (2007).

[57] See Supplemental Material at http://link.aps.org/supplemental/10.1103/PhysRevB.95.121410 for details of the calculations.